*J. Fluid Mech.* (1985), *vol.* 151, *pp.* 219–241
*Printed in Great Britain*



# The development and structure of primary and secondary flow in a curved square duct

By P. HILLE, R. VEHRENKAMP† AND E. O. SCHULZ-DUBOIS
Institute of Applied Physics, University of Kiel, F.R. Germany

(Received 19 December 1983 and in revised form 8 August 1984)

The development of laminar flow in a 180° section of a curved square duct ($R/d = 6.45$) was studied by laser-Doppler anemometry (LDA). The streamwise flow-velocity component $V_\phi$ and the secondary flow component $V_r$ were measured as a function of Dean number and of the azimuthal angle $\phi$. The development of the streamwise flow component was found to be connected with a strong momentum transfer towards the outer wall between $\phi = 0°$ and $\phi = 60°$, with a partial back-transfer of the momentum towards the duct centre ($\phi = 45°$–$108°$), and with little further change of the momentum between $\phi = 108°$ and 180° near the outer wall. The measurements of the $V_r$ component showed at least one vortex pair in the secondary flow. A second vortex pair with opposing sense of circulation was found to develop near the outer wall only for Dean numbers between 150 and 300, in agreement with numerical calculations. This second vortex pair was found in the region between $\phi = 108$ and 171°. Between $\phi = 60$ and 108° it was not possible to identify the second vortex pair in the developing flow. However, developing laminar-flow numerical calculations by Humphrey (1982) show that it also arises for $K = 485$ in a 180° square duct with $R/d = 3.35$ and $Re = 890$, and it is a function of inlet flow conditions. From the measured stream-function maximum of the second vortex pair it may be deduced that a curved duct with 180° (20 hydraulic diameters) bend angle is not sufficient to reach fully developed flow conditions at $d/R = 1/6.45$ and $K = 226$.

## 1. Introduction

Viscous flow through straight ducts of various cross-sectional forms is well understood. The development of the asymptotic flow from a uniform distribution of axial velocity at the inlet is accounted for by boundary-layer theory (Schlichting 1934).

The flow in a gently curved duct may be considered as a modification of straight laminar flow in which the effects of centrifugal forces must be considered (Dean 1928*b*). An extended review of curved pipe flow was made by Berger, Talbot & Yao (1983). They discuss the entry flow and the fully developed laminar flow, and point out that both depend on two parameters, namely curvature ratio and Dean number. (Henceforth we will use $d$ for the hydraulic diameter $2ab/(a+b)$, $a$ and $b$ for the inner width and height of the duct, $\gamma$ for the curvature ratio $\gamma = d/R$, and $K$ for the Dean number $Re(d/R)^{\frac{1}{2}}$. $R$ is the duct curvature radius, and the Reynolds number is calculated with the average mainstream velocity $\overline{V_\phi}$, $Re = \overline{V_\phi}\, d/\nu$, where $\nu$ is the kinematic viscosity.) The Dean number and curvature are necessary parameters for

† Present address: Lambda-Physik, D-3400 Göttingen, F.R. Germany.

the characterization of a curved duct flow, and only for small curvature ratios may the influence of $\gamma$ on the flow be neglected.

Most numerical computations are restricted to fully developed curved-duct flow. To compare the results of such computations with experiments, one would have to know whether or not the experimental flow is fully developed. Knowledge of the development and structure of primary and secondary flow in curved pipes is helpful in practical applications, for example in the design of heat exchangers. Furthermore, the flow in some curved geometries shows hydrodynamic instabilities. Dean (1928*a*) found such an instability in curved infinitely high channels, and Benjamin (1978) applied the concepts of bifurcation theory to flows in finite geometries. Therefore the question arose as to whether the flow phenomena in curved ducts could be interpreted as instabilities.

Recent secondary-flow measurements in curved pipes were made by Olson (1971) with pulsed hot-wire equipment and by Agrawal, Talbot & Gong (1978) with laser-Doppler anemometry. Both studies found that the development of the entry flow is associated with the generation of axial vorticity; this leads to growing vortices, while continuity is not conserved in the cross-section. In addition Agrawal *et al.* found more involved flow patterns at higher Dean numbers (e.g. $K = 678 \times 2^{\frac{1}{2}}$) and for $\phi = 50°$–$105°$ ($d/2R = \frac{1}{7}$, between $2L/d = 6.11$–$12.83$, with $L \equiv$ entrance length). They identified them as consisting of two vortex pairs, the weaker one located near the inner wall. Humphrey (1978) and Humphrey, Chang & Modavi (1982) found such a four-vortex pattern in their numerical analyses of developing flow in a circular pipe and in a 180° curved duct of square cross-section respectively, but they found it at the outer wall (see Appendix III of Humphrey *et al.* 1982).

For curved square or rectangular channels, the theoretical treatment is involved, since the required eigenfunctions are not available in analytical form. Numerical calculations by Cheng, Lin & Ou (1976), Ghia & Sokhey (1977) and Joseph, Smith & Adler (1975) on fully developed flow in a curved square duct predict the existence of a second weak vortex pair near the outer wall. Its sense of rotation is opposite to that of the bigger pair. Cheng *et al.* (1976) found the second vortex pair at Dean numbers higher than $K = 150$ (different curvatures, see table 1 for comparison). The additional vortex pair was also found in the calculations of Ghia & Sokhey, who gave a lower limit of $K = 143$ for its onset, and in calculations of Joseph *et al.* for $K > 152$ (related to $d$). Indeed there was no evidence of a second vortex below $K = 150$ in this experiment, as in all previous experiments. For higher Dean numbers around $K = 500$ there are contradictory results concerning the additional vortex pair in numerical calculations. Cheng *et al.* (1976) found indications that there is no extra pair at the Dean number $K = 520$ and $\gamma = \frac{1}{4}$ (developed flow), while Humphrey *et al.* (1982) obtained the extra pair for developing flow in a 180° curved duct of square cross-section with $K = 485$ and $\gamma = 1/3.35$ in a similar way as at lower Dean numbers. The strength of the calculated vortex pairs depends on the entry profile (flat or parabolic) according to the results of Humphrey *et al.* (1982, Appendix III). The question remains at what curvature ratios and in what range of higher Dean numbers the additional pair may exist and up to what azimuth the entry flow influences the onset of that pair.

Nandakumar & Masliyah (1982) discussed the instability aspects of the additional secondary vortex pair. They interpreted the appearance of different flow solutions in curved pipes as a bifurcation phenomenon in the sense used by Benjamin (1978). In curved pipes and in semicircular-cross-section geometries Nandakumar & Masliyah found a bifurcation of the two-vortex solution into a two- and a four-vortex solution at $K = 100$. They analysed the attraction of the four-vortex solution in terms of

cross-section shape and Dean number. They found that the four-vortex solution is much easier to obtain if the outer wall profile is flat.

A treatment of the developing flow in the entry section of curved pipes or ducts would be necessary to predict the run length needed for the development of the flow. Singh (1974), Smith (1976) and Yao & Berger (1975) treated the entry-flow problem by means of three-dimensional boundary-layer theory. Smith's analysis includes an upstream response (in the straight section) to downstream pressure variations (in the bend). He found that the larger wall shear stress occurs at the inside in the entry part of the bend, but from 1.51 radii onwards the larger shear stress occurs at the outside; at the point of crossover the centrifugal and inertial forces are equally strong. The calculations of Smith are in agreement with the experiments of Agrawal *et al.* (1978) and Olson (1971) for the flat entry-flow profile. In this case a shear-stress crossover was found by Olson at $\phi = 20°$ (5 radii) in the bend ($K = 407 \times 2^{\frac{1}{2}}$, $R/d = 8.0$).

However, in the experiments with fully developed entry-flow profile (Olson 1971; Humphrey, Taylor & Whitelaw 1977), as well as in the present work, this crossover was not found, because the boundary layer is already large. Instead it was found that the velocity maximum is always closer to the outside wall, and that the larger shear stress occurs at the outside wall. In fact, the velocity maximum moves monotonically toward the outside wall up to $\phi = 60°$. For a strongly curved rectangular duct, $d/R = \frac{1}{2}$, Humphrey *et al.* (1977) found a region of streamwise flow reversal near the outer wall at the bend inlet which is the result of the initial strong deceleration there.

Experimental results by the authors mentioned indicate a transfer of streamwise momentum associated with a displacement of velocity maximum towards the outer wall up to $\phi = 60°$. Between $\phi = 45°$ and about 110° the momentum is partially transferred back towards the inner wall. While the transfer of momentum density towards the outer wall (between $\phi = 0°$ and 60°) is due to the change of the geometry from a straight section to a curved section, the momentum density increase between midplane and inner wall (between $\phi = 45°$ and 110°) is coupled with fluid transport by the developing secondary flow; more fluid is transported by the first vortex pair back towards the inner wall than from the region between the inner wall and the duct centre to the outer wall. According to Olson (1971), we may call the momentum transfer to the inner wall an 'overshoot'. Past the transient region, i.e. past about 110°, the flow would seem almost developed, since little change in the mainstream-velocity component $V_\phi$ can be detected experimentally. As we will show by our measurements of secondary flow, the flow development is not complete up to 180° (that is, about 20 hydraulic diameters away from the inlet) for a curvature ratio $d/R = 1/6.45$. This is in agreement with the calculations of Humphrey *et al.* (1982) for $d/R = 1/3.35$.

Somewhat related to our experiments is a combined theoretical and experimental study by Mullin & Greated (1980), who investigated the problem of oscillatory flow in curved pipes. Further experiments on pulsating flow in curved pipes were carried out by Talbot & Gong (1983), who found separation during the decelerating phase of the cycle (for new work on oscillatory flow see also Bertelsen 1983).

## 2. Experimental set-up

The test section of our experimental set-up is shown schematically in figure 1. It consists of 180° bend of a square-cross-section channel with a hydraulic diameter of 3.8 cm and of straight inlet and outlet sections. An inlet section of 2 m was chosen (52 times the hydraulic diameter), which was longer than that required for full

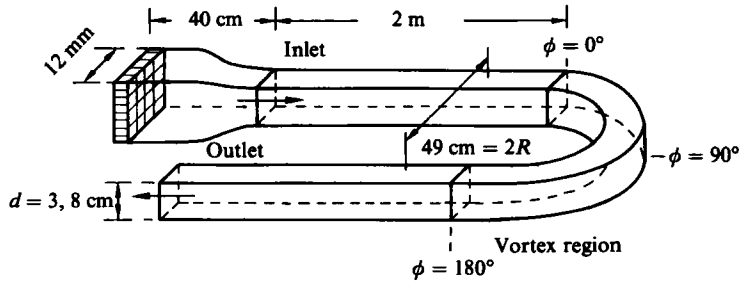


FIGURE 1. Geometry, dimensions and arrangement of the curved square duct. The straight inlet tubes force a fully developed inlet profile and prevent upstream influences from the system outlet. The inlet into the straight section is conditioned with a calming chamber and a honeycomb grid.

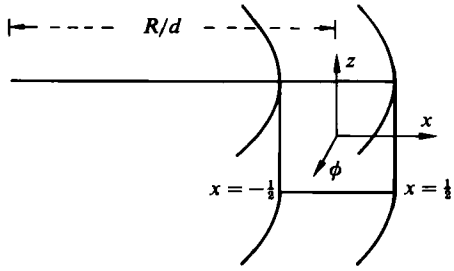


FIGURE 2. Coordinates of the curved square-channel section. The radial component is defined as $x = (r-R)/d$, with $d \equiv$ hydraulic diameter and $R \equiv$ radius of curvature. The velocity in the $x$-direction is denoted by $V_r$.

development of the laminar profile (Schlichting 1934) at the highest Reynolds number occurring in this experiment. The channels were made of transparent Lucite (Plexiglas) to facilitate laser-Doppler anemometry (LDA) measurements. At the same time, this material has a low heat conductivity, which helps to suppress unwanted thermal-buoyancy effects in the working fluid.

The system of coordinates used for the description of the curved duct section is shown in figure 2. The bend had a curvature ratio $d/R = 1/6.45$. Note that the dimensionless cross-section coordinates are denoted by $x$ and $z$. They both vary between $-\frac{1}{2}$ and $\frac{1}{2}$.

For a non-isothermal working fluid, buoyancy effects may cause a secondary flow which may mask the object of our study, i.e. the secondary flow due to centrifugal effects.

The influence of temperature gradients on the flow through straight and curved pipes has been studied by several authors for either uniform-heat-flux or uniform-wall-temperature boundary conditions (Cheng *et al.* 1974; Cheng, Hong & Hwang 1972; Mori & Futagami 1967; Scheel & Schulz-DuBois 1982). Summarizing the published numerical results and some experimental results in the straight section of a rectangular curved duct (Vehrenkamp 1980; Augustin 1982), a Rayleigh number $Ra = 10000$ causes secondary flow velocities with a magnitude of 1 % (2.5 %) of the mainstream velocity for Reynolds numbers larger than $Re = 400$ (200).

For our curved square duct with a cross-sectional dimension of 3.8 cm, with water as working fluid and temperature control within $\pm 0.01$ K, we obtain a Rayleigh number $Ra = gBd^3\Delta T(\nu\alpha)^{-1} = 9800$ ($d \equiv$ hydraulic diameter, $B \equiv$ coefficient of thermal expansion, $g \equiv$ gravitational acceleration, $\alpha \equiv$ thermal diffusivity, $\nu \equiv$

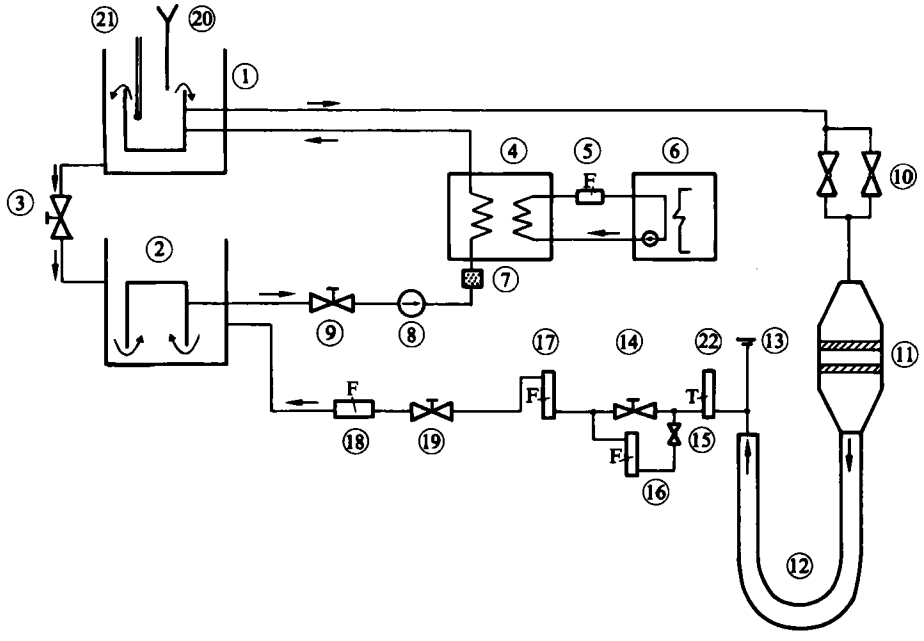


FIGURE 3. Experimental setup of the flow system: 1, upper overflow reservoir; 2, lower underflow reservoir; 3, overflow stopcock; 4, heat exchanger/Alpha Laval type DO; 5, flowmeter 3000 l/h; 6, thermostat with pump/Lauda tupe RC20; 7, filter; 8, pump 30 W/type Eheim 1026; 9, pump-system stopcock; 10, flow regulator; 11, flow-calming chamber; 12, duct system; 13, ventilation; 14, bypass; 15, flow regulator (used at low Dean numbers, smaller than 100; 16, flowmeter up to 30 l/h ($K = 100$)/Brooks Shorate; 17, flowmeter up to 300 l/h/Brooks DD1120; 18, flowmeter 3000 l/h; 19, duct-system stopcock; 20, seeding injection; 21, NTC thermometer $\frac{1}{1000}$ °C; 22, thermometer $\frac{1}{100}$ °C.

kinematic viscosity, and $T \equiv$ temperature). The velocity of the buoyancy-driven secondary flow then has a magnitude of 100 μm/s; this is about 1 % of the streamwise velocity for a Reynolds number $Re = 556$.

The combined hydraulic-flow and temperature-control system is shown in figure 3. The water temperature was held constant to within ±0.01 °C for several hours, while the laboratory air was controlled to within ±0.5 °C. Thus it was possible to reduce the Rayleigh number to below $10^4$. The control system involved several thermistors, electric heating elements and a counterflow cooler using tap water. The flow system was covered with polystyrene foam for thermal insulation. Windows were inserted where laser-Doppler measurements were intended. The room temperature was kept somewhat above that of the rest of the building. In principle, temperature-control requirements could be diminished by use of a duct with smaller cross-section. But this would lead to a reduced relative spatial resolution of the LDA measurements. The selected size of $(38\text{ mm})^2$ corresponds to about $100 \times 100$ resolvable points.

For a cross-section of this size the relevant velocities, in particular the radial component, are of the order of 0.1–2 mm/s, and hence difficult to measure. To overcome this problem we developed suitable laser-Doppler and data-extraction methods (Hille, Vehrenkamp & Schulz-DuBois 1983) based on photon-correlation techniques and a refined fast-Fourier-transformation algorithm. An LDA system is preferred because the measurement is non-intrusive and strictly yields a Cartesian velocity component even if the measured component is small compared with the

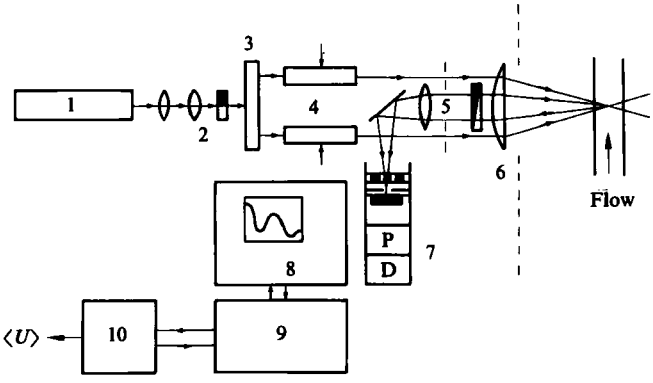


FIGURE 4. Laser-Doppler anemometry system and data-processing system. The diameter of the measuring volume was about 50 μm, the fringe distance was 2.48 μm. 1, He–Ne laser; 2, optic with half-wave plate; 3, beam splitter; 4, Bragg cells; 5, receiving optic; 6, lens; 7, photomultiplier system (D, discriminator; P, photomultiplier); 8, correlator; 9, microprocessor (fast Fourier transform); 10, terminal.

dominant velocity component. Similar measurements with pulsed hot-film techniques require a considerable effort (Olson 1971).

To maintain a constant pressure difference between inlet and outlet and to avoid pressure pulsations inherent in all types of pumps, an overflow system was used. Two reservoirs were positioned at fixed heights above and below the channel. In the upper one the water level was kept constant by an overflow outlet.

In the curved channel section the laser-Doppler system shown in figure 4 was used. By rotating its optical part by 90° this system can be set up to measure either the main, azimuthal velocity component $V_\phi$ or the secondary, radial component $V_r$. To achieve better mechanical stability of the optical system, a backward-scattering system was used. With this set-up vertical profiles $V_\phi(z)$ or $V_r(z)$ could be measured at radial positions. Thus it was possible to obtain data about the entire field $V_r(x, z)$ at a given azimuth $\phi$. Note that velocity measurements close to the walls (1–3 mm) were not possible owing to the slant of the laser beams and to water–Lucite interface reflections. These reflections caused too strong photon noise, which prevented measurements.

The laser-Doppler measuring volume had a diameter of 50 μm (in the $(x, \phi)$-plane) and a length of 0.4 mm (in the $z$-direction). The angle between the laser beams was 14.66°, leading to a fringe distance of 2.48 μm. For measurement of the small radial velocity component $V_r$ a comparatively low Bragg-shift frequency of 12 kHz was used. The main velocity $V_\phi$ was measured without Bragg shift.

Photon correlation was used for laser-Doppler signal analysis because the backscattered light intensity is small. In addition it offers the advantage of obtaining velocity data whose accuracy may be enhanced by a longer sampling period. The laser-Doppler signal was fed to a Malvern K7023 photon correlator having 96 channels. The sample time (time delay between two channels) was 10 μs, leading to a total time lag of 960 μs. In our studies a sampling period of 45 s proved adequate for determination of a velocity value which involved the correlation and subsequent fast Fourier transformation followed by an interpolation algorithm. Owing to the symmetry of the photon autocorrelation function, 192 channels were used in the Fourier transformation. The interpolation algorithm (Hille *et al.* 1983) led to a resolution in the velocity values that is 50 times better than that due to the Fourier

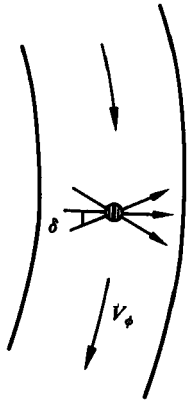


FIGURE 5. With tilted measurement set up, not only the secondary-flow component $V_r$ is measured, because a systematic error $\delta V_\phi$ is added.

transform alone. In this way the velocity was determined with an absolute error of 20 μm/s only.

For the determination of the radial velocity $V_r$ the orientation of the laser cross-beam pattern is crucial. If there is a misalignment around the optical axis of $\delta$ (see figure 5) the measured component is

$$V_m = V_r \cos\delta + V_\phi \sin\delta, \tag{1a}$$

which gives

$$V_m = V_r + V_\phi \delta \quad \text{for small } \delta. \tag{1b}$$

Since $V_\phi/V_r$ may be 30, the permissible misalignment for a less than 3% error is $\delta < 10^{-3} = 3.6$ minutes of arc. Instead of alignment by purely geometrical means, we made use of development and symmetry properties of the flow itself. For a fully developed laminar flow the continuity equation applies in the two dimensions of cross-section. The secondary flow may hence be described by a stream function, and, in particular, the integral

$$I(x) = \int_{-\frac{1}{2}}^{+\frac{1}{2}} V_r(x,z)\,\mathrm{d}z = 0 \quad \text{for } -\tfrac{1}{2} < x < \tfrac{1}{2} \tag{2}$$

vanishes when the flow is fully developed. In the alignment procedure $\delta$ is varied until the integral over the component $V_m$ vanishes. This was possible between $\phi = 108°$ and 162° (see figure 8). Note that the integral (2) does not vanish for some $x$ if the flow is not fully developed, i.e. if the mean-velocity component still undergoes changes in the streamwise direction ($\partial V_\phi/\partial\phi \neq 0$). In this case (2) becomes

$$I(x) = \int_{-\frac{1}{2}}^{+\frac{1}{2}} \int_{R+x}^{R+\frac{1}{2}} \frac{1}{r}\frac{\partial V_\phi}{\partial\phi}\,\mathrm{d}z\,\mathrm{d}r. \tag{3}$$

From the streamwise flow profiles (figure 6) we obtained the change for $V_\phi$ of $8 \times 10^{-3}$ cm/s within $\Delta\phi = 1°$ in the region with the best streamwise flow development (that is the region between $\phi = 108°$ and 162°). Therefore, applying the continuity equation, at the radial position $x = 0.29$ (0.8 cm away from the outer wall) the error for $I(x)$ is calculated to be 0.06 cm²/s. This is in agreement with the direct measurements of $I(x)$ (figure 8). The resulting velocity error due to an alignment procedure in the region between $\phi = 108°$ and 162° is therefore less than 150 μm/s. After alignment, $I(x)$ is indicative of the degree to which the flow has developed.

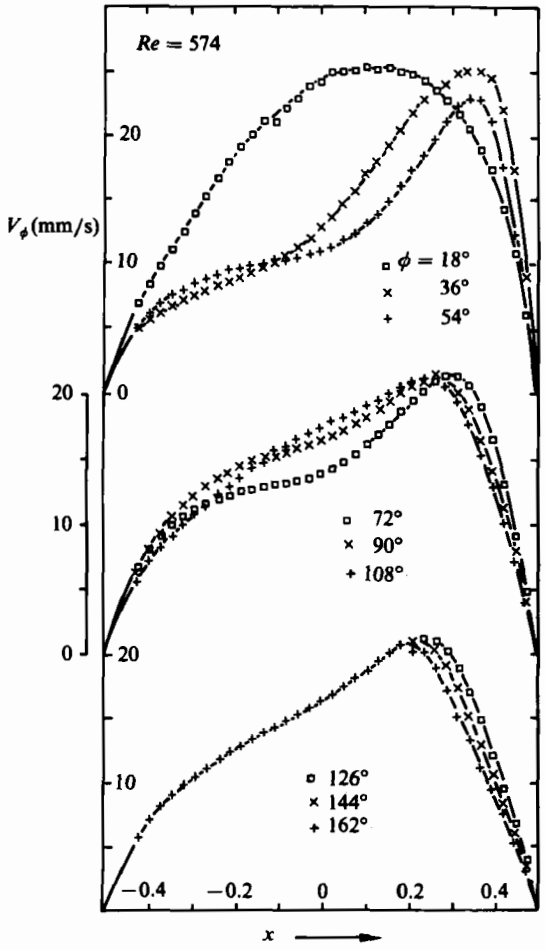


FIGURE 6. Mainstream velocity as a function of the radial location $x$ at $z = 0$ and $K = 226$. The measurements are taken at various points around the bend.

## 3. Experimental results

Measurements of the main azimuthal velocity component $V_\phi$ were taken in order to obtain information on flow development. $V_\phi$ was measured as a function of the radial coordinate $x$ in the midplane of the cross-section, $z = 0$, at intervals of 18° in the azimuthal angle. These data were all recorded at a Reynolds number $Re = 574$ with a corresponding Dean number $K = 226$ ($R/d = 6.45$). These results are shown in figure 6. The midplane velocity maximum, initially located at $x = 0$ in the straight inlet section, gradually moves outward, and reaches $x = 0.35$ near $\phi = 36°$. It remains there up to $\phi = 54°$. For $\phi > 54°$ the maximum velocity is slightly reduced. Obviously the strong flow near the outer wall is due to a tendency for conservation of the initial linear flow momentum at the inlet.

For azimuthal angles between $\phi = 45°$ and 108° the midplane streamwise flow velocity increases between the channel centre and the inner wall at $x = -0.3$ (figure 6). We recognize that the increasing velocity near the inner wall is part of the overshoot mechanism. It is coupled with a decrease of the mass flux in the outer-wall

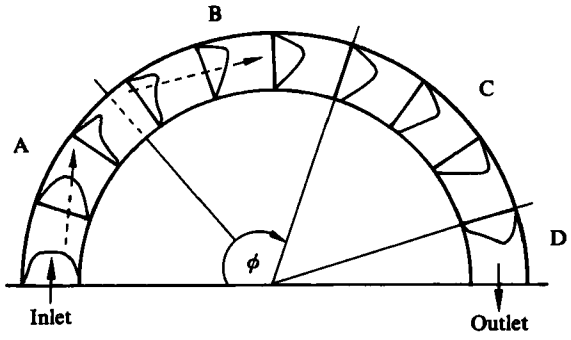


FIGURE 7. Streamwise velocity development. Shown is $V_\phi$ in the midplane of the curved channel. A, entry flow; B, overshoot region; C, fully developed region; D, outlet region. The measurements shown in figure 6 are sketched.

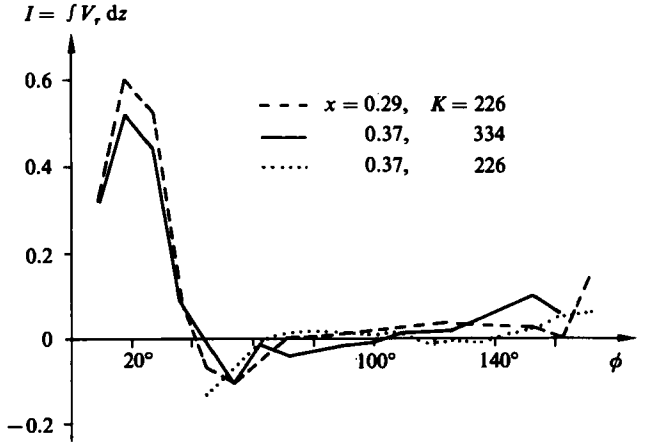


FIGURE 8. Influence of the streamwise velocity on the radial velocity as a function of the azimuthal angle. Non-zero integral $I$ may either mark a non-fully developed flow or an error in the adjustment. A positive integral is due to mass transfer to the outer wall if the measurement set-up is properly adjusted.

region, and a non-zero mass flux from the outer wall to the inner wall in the radial direction. The mass flux in radial direction is indicated in figure 8. Between $\phi = 45°$ and 70° we obtain a negative integral of the radial velocity along a vertical location (see also figure 7). Further curves in figure 6 show that the streamwise velocity does not change noticeably with $\phi$ in the region between $x = -0.5$ and 0.2. This suggests that in the region $108° < \phi < 162°$ the inner part of the flow pattern is practically fully developed or better; changes are smaller than measurement uncertainties. This fact is corroborated by data on the primary vortex pair. On the other hand, near the outer wall, $0.2 < x < 0.5$, the curves of figure 6 ($\phi = 126°$–$162°$) show a slight rearrangement of the flow maximum towards the inside, a trend that points to the influence of the second vortex pair. This suggests that the flow is not fully developed if we take the small changes of the second vortex pair into account. In figure 7 the streamwise flow development is summarized.

Further information on the question of the flow development is presented in the data of figure 8, where the integral over the radial velocity given by (3) is evaluated

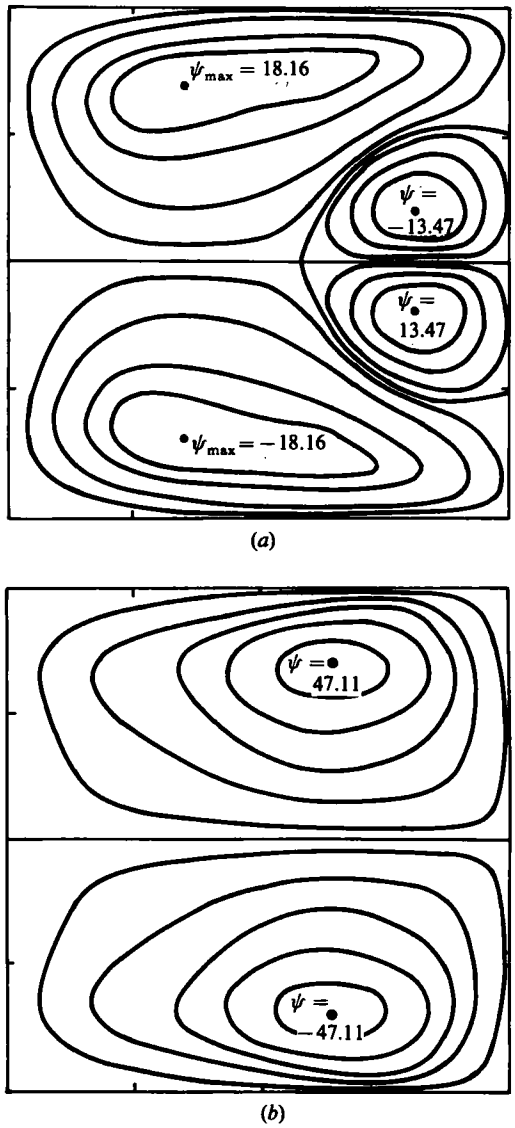


FIGURE 9. Numerical results for secondary-vortex structure (after Cheng *et al.* 1976). The qualitative agreement with figure 10 is obvious. For quantitative comparisons see table 1. (*a*) $R/d = 10$, $K = 368$; (*b*) $R/d = 4$, $K = 520$.

numerically from measured data and is plotted versus $\phi$ for the indicated radial coordinates $x$. There are two regions where the integral $I(x)$ does not vanish, thus indicating radial mass flux. Up to $\phi = 45°$, where $I$ is positive, it is known from the mainstream velocity measurements that the maximum moves toward the outside. At $\phi = 45°$, $I$ vanishes, but this may not be taken as a sign for fully developed flow since $\mathrm{d}I/\mathrm{d}\phi \neq 0$. From $\phi = 45°$ up to a value near 80° or 90°, $I$ is negative, and this is known to be related to the overshoot. From there on, the plotted values of $I$ are equal to zero, with a margin of error of 0.05 cm$^2$/s. This indicates a velocity error of 130 μm/s due to improper adjustment.

The next results are concerned with the appearance of a second vortex pair. For

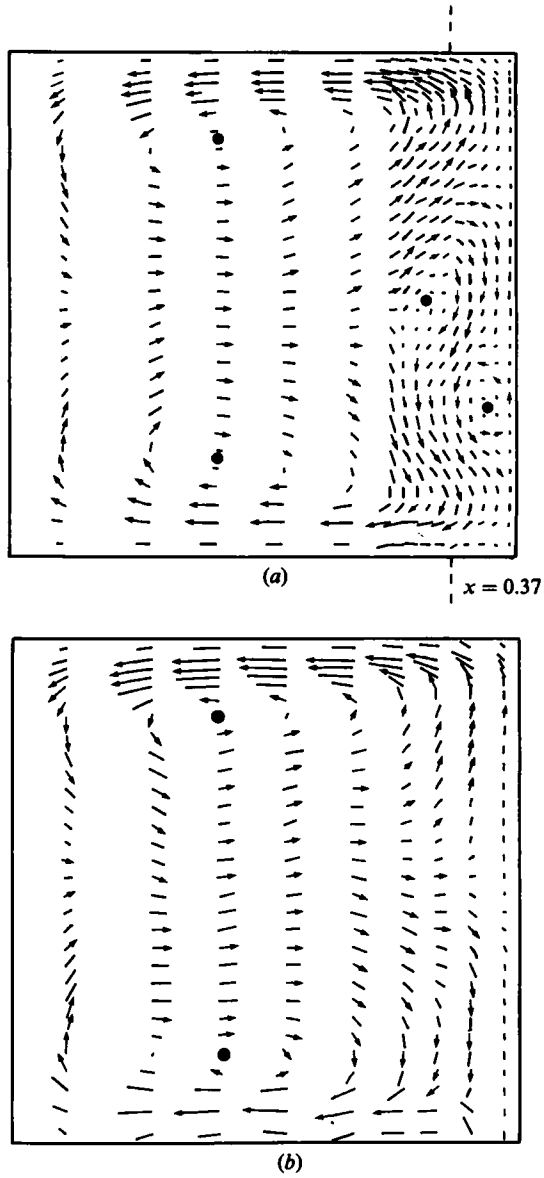


FIGURE 10. Two-dimensional profiles of secondary velocities (radial velocity component $V_r$ measured, vertical velocity component $V_z$ reconstructed, see text). In (*a*) four vortices may be recognized. The additional vortex pair near the outer wall is asymmetric. The additional vortex pair disappears at higher Dean numbers $K > 300$ (*b*). (*a*) $\phi = 136°$, $K = 226$, $Re = 574$; (*b*) $\phi = 136°$, $K = 334$, $Re = 853$; both have $R/d = 6.45$.

a wide range of Reynolds or Dean numbers, the secondary flow pattern looks similar to figure 9(*b*) computed by Cheng *et al.* (1976) for a developed flow at $K = 520$, $d/R = \frac{1}{4}$: the main feature is a pair of primary vortices created by centrifugal effects in the centre of the cross-section. For a limited range of conditions, for example $K = 368$, $d/R = \frac{1}{10}$, they calculated patterns like figure 9(*a*), which features a second vortex pair and a free stagnation point. If one considers the transfer of streamwise momentum by the secondary flow pattern of figure 9(*a*), it is apparent that the

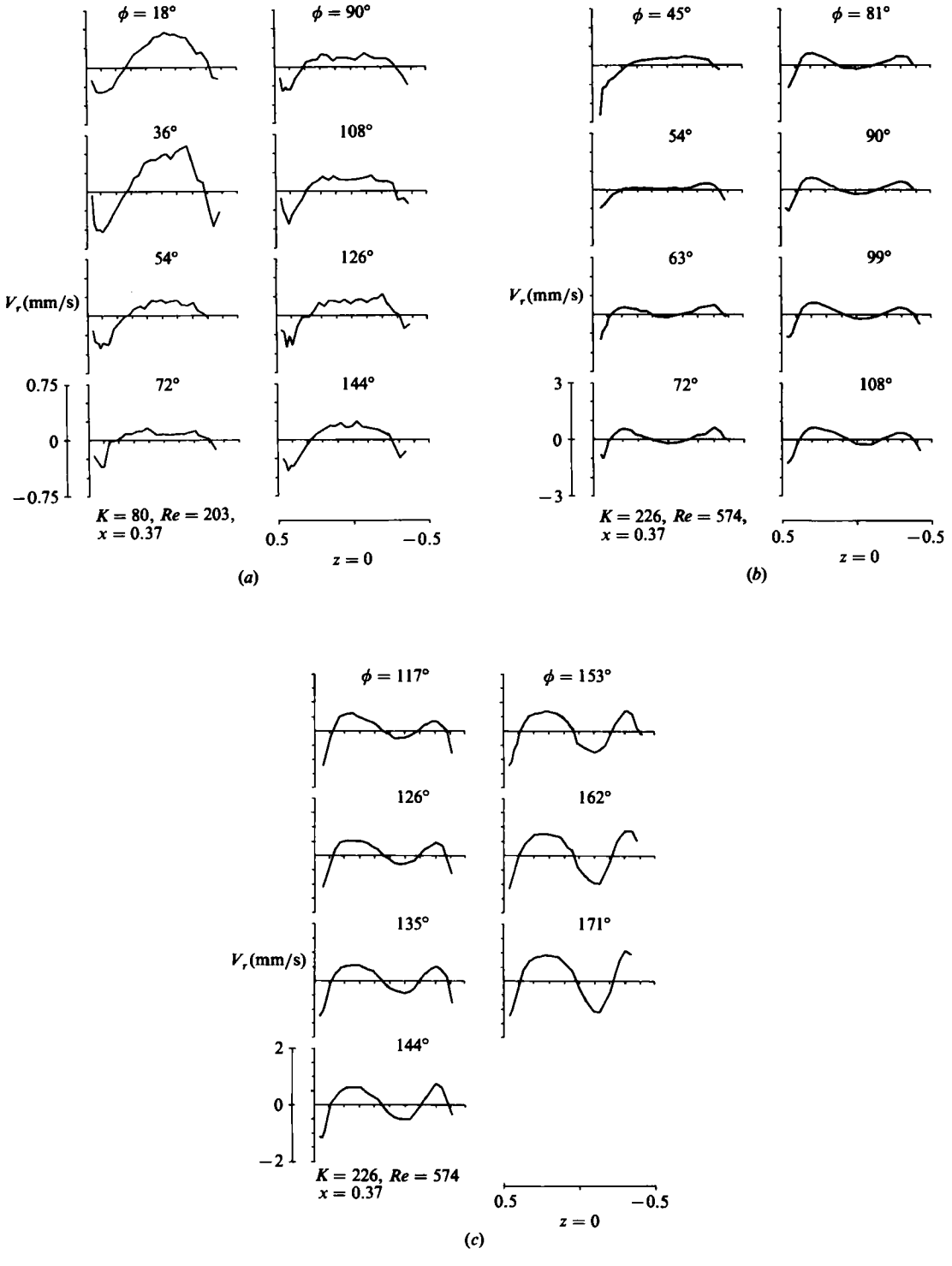


FIGURE 11. (a–c). For description see opposite page.

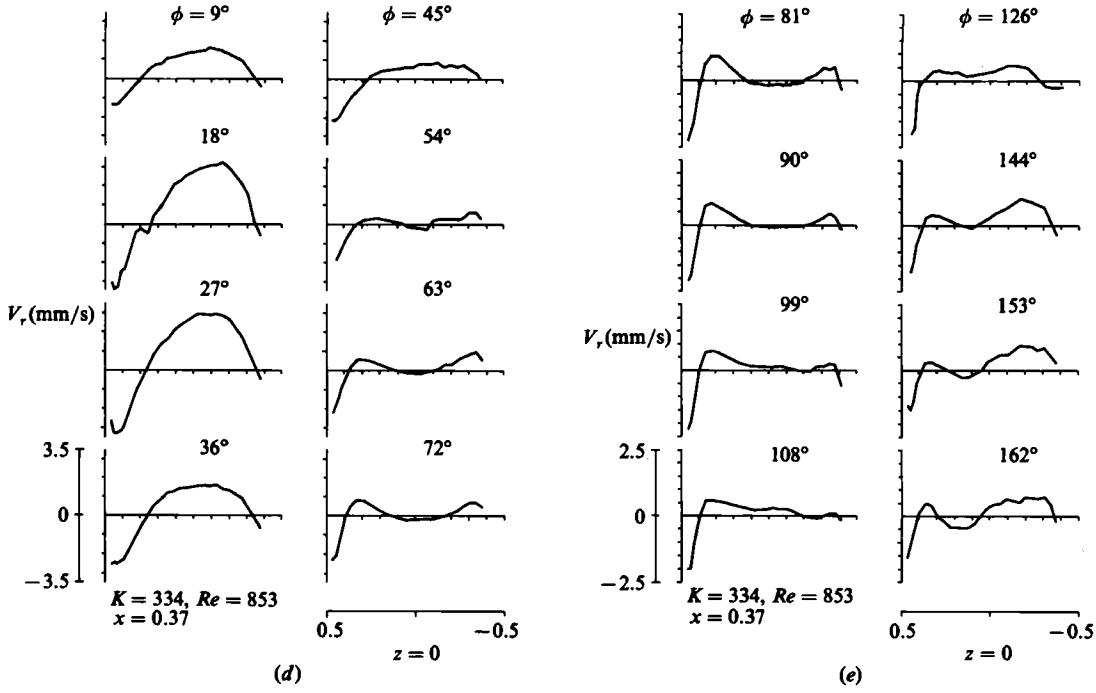


FIGURE 11. Measured secondary-velocity profiles of the radial velocity component $V_r$ in dependence of vertical location $z$: (*a*) secondary flow at a low Dean number $K = 80$; (*b*), (*c*) Dean number $K = 226$ – an additional velocity minimum indicates an additional vortex pair; (*d*), (*e*) at higher Dean numbers there is no additional vortex pair in the region between $\phi = 110°$ and 150°. The measured negative velocities $V_r$ between $\phi = 54°$ and 108° are due to non-fully developed entry flow; between $\phi = 150°$ and 180° an upstream influence from the outlet disturbs the flow.

additional vortex pair tends to repel the maximum of the streamwise velocity from the outer wall. Thus the second vortex pair seems necessary in order to keep the velocity maximum closer to the centre of the cross-section, which in turn reduces viscous friction.

For two flow conditions, $K = 226$ and $K = 334$, both at $\phi = 136°$, we have determined the entire secondary flow pattern shown in figures 10(*a*, *b*). The quantity used to determine these patterns was $v_r$ measured at numerous points in the $(x, z)$-plane. Since the flow may be considered as fully developed within the required numerical accuracy, the two-dimensional continuity equation holds. We then obtained $v_z$ through numerical integration, including interpolation to obtain the near-wall points, and differentiation:

$$V_z(x,z) = -\int_{-\frac{1}{2}}^{z} \left( \frac{\partial V_r(x,z')}{\partial x} + \frac{V_r(x,z')}{x + d/R} \right) \mathrm{d}z. \tag{4}$$

In figure 10(*a*), besides the two big primary vortices with centres at coordinates $x = -0.09, z = \pm 0.30$, one recognizes at least one small vortex with centre at $x = 0.33$, $z = -0.03$: a slight asymmetry in the $V_r$ profiles, and consequently in the vortex structure, made its counterpart too small for easy identification. In figure 10(*b*), by contrast, there are two main vortices, without a trace of a second vortex pair.

As a check on the presence of the additional vortex pair, we measured vertical profiles of $V_r$, $V_r(z)$ at $x = 0.37$ close to the outer wall – see the dashed line in figures

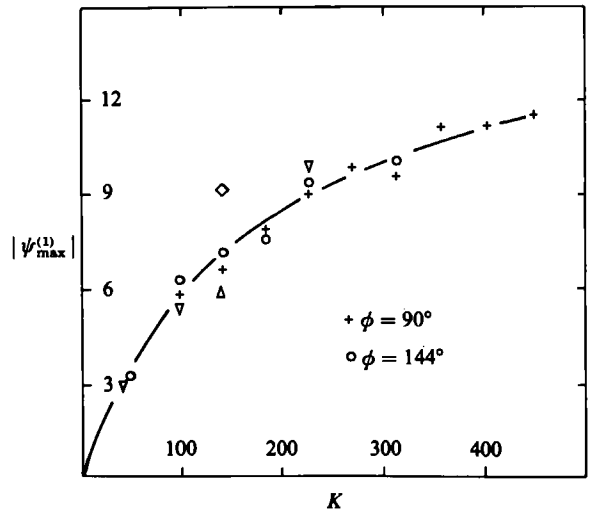


FIGURE 12. Dean-number dependence of the first vortex pair. $\psi^{(1)}_{max}$ is the value of the dimensionless stream function in the vortex eye. +, $\phi = 90°$; ○, $\phi = 144°$, numerical results: △, Ghia & Sokhey (1977), ◇, Cheng *et al.* (1976); ▽, Joseph *et al.* (1975).

10(*a*, *b*). If there is no additional vortex pair the radial velocity is positive, i.e. towards the outside, at vertical location $z = 0$. If there is a second vortex pair, the velocity $V_r$ is negative near $z = 0$. Keeping this in mind, the data of figure 11 (*a*) show that there is no second vortex pair at $Re = 203$, $K = 80$. As figures 11 (*b*, *c*) show, however, at $Re = 574$, $K = 226$ there is a second vortex pair starting at about $\phi = 60°$; the inward flow between these extra vortices has a negative velocity $V_r$. The additional vortex pair is present for $\phi > 60°$. At still higher flow rates $Re = 853$, $K = 334$, as seen in figures 11 (*d*, *e*), there is a weak indication of the additional vortex pair between $\phi = 54°$ and 90°, and from 90° to 144° there is uncertain indication of these vortices. The negative velocity $V_r$ indicates the existence of the additional vortex pair certainly, if the flow is fully developed and if $I(x) = 0$ ($\phi = 108°$–144°). If $I$ is not zero, it is not possible to separate developing flow and secondary vortices. Therefore we conclude from figures 10(*a*, *b*) that there is no additional vortex pair at $K = 334$ and that there is an additional vortex pair at $K = 226$.

We have used the value of the dimensionless stream function in the eye of the respective vortex to obtain a quantitative comparison of calculated flows with the experimental data. By definition, the stream function has an extremum there. This may be computed from measured data by numerical integration:

$$\psi_{max} = \frac{1}{\nu} \int_{-\frac{1}{2}}^{z_0} V_r(x_0, z)\, dz \tag{5}$$

where $(x_0, z_0)$ is the location of the vortex eye. Figure 12 shows the maximum of the stream function of the primary vortex as determined from our measurements at 10 different Dean numbers and two azimuthal angles in the developed range. $\psi_{max}$ is the same for both angles, and it is a monotonically increasing function of the Dean number, roughly proportional to $K^{\frac{1}{2}}$. Also shown in figure 12 is a calculated value by Cheng *et al.* (1976), which is about 25% greater than our experimental data, and two calculated values by Ghia & Sokhey (1977), which differ by ±10% from the experimental data. A similar plot of the stream-function maximum for the second

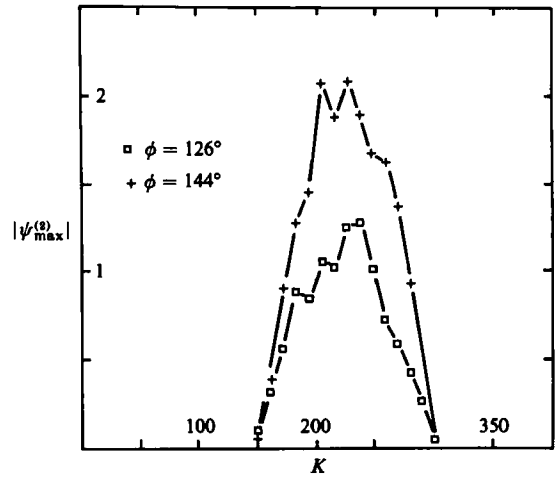


FIGURE 13. Dean-number dependence of the additional vortex pair. $\psi^{(2)}_{max}$ is the dimensionless stream function in the vortex eye. The vortex pair appears at $K = 150$ and disappears at $K = 300$.

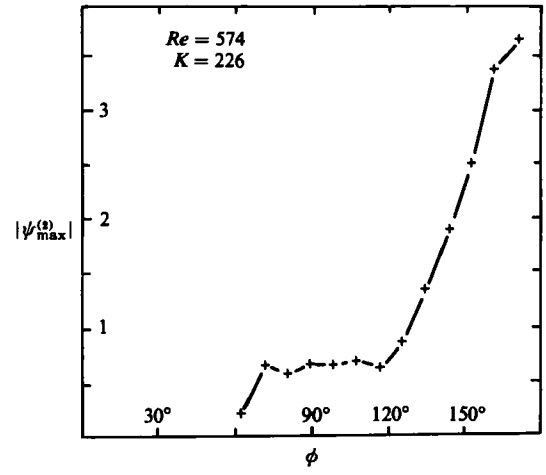


FIGURE 14. Development of the additional vortex pair in dependence of the azimuthal angle. The vortex strength increases after $\phi = 110°$; in this region the streamwise flow is practically fully developed. Obviously an angular dependence of interaction between additional vortex pair and streamwise flow leads to an increasing second vortex-pair strength for $\phi > 110°$ (see figure 6 for comparison).

vortex pair is shown in figure 13. These values, evaluated from the measurements, are an order of magnitude smaller than those of the primary vortex pair. The stream-function values for $\phi = 144°$ are greater than those at $\phi = 126°$ (by a factor of around 1.6). The most interesting feature is the fact that there is no additional vortex pair for Dean numbers either smaller than 150 or larger than 300. In the range $150 < K < 300$ the 'strength' of the second vortex pair passes through a maximum.

Figure 14 shows the maximum of the experimentally determined stream function of the additional vortex pair as a function of the azimuthal angle at fixed $Re = 574$, $K = 226$. Here the quantity $\psi^{(2)}_{max}$ is constant only in the range $68° < K < 125°$, while for larger angles it increases greatly. This suggests that the fully developed value of

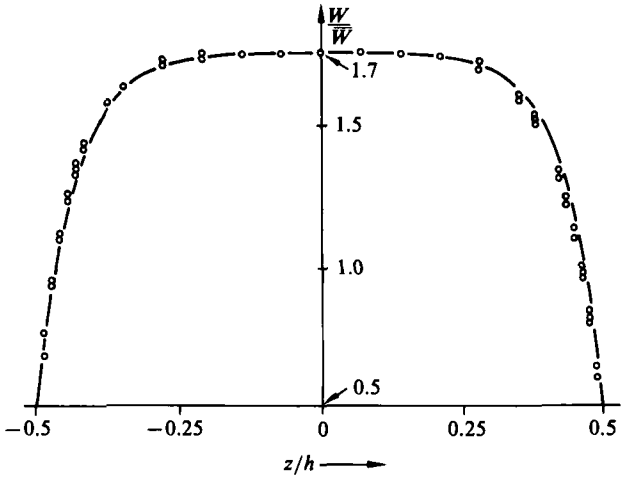


FIGURE 15. Streamwise velocity as function of vertical location $z$. This profile was measured in the straight inlet tube of a rectangular curved square channel with an aspect ratio $h/w = 5/1$ at $Re = 10000$. ○, experimental result; ——, theoretical flow solution.

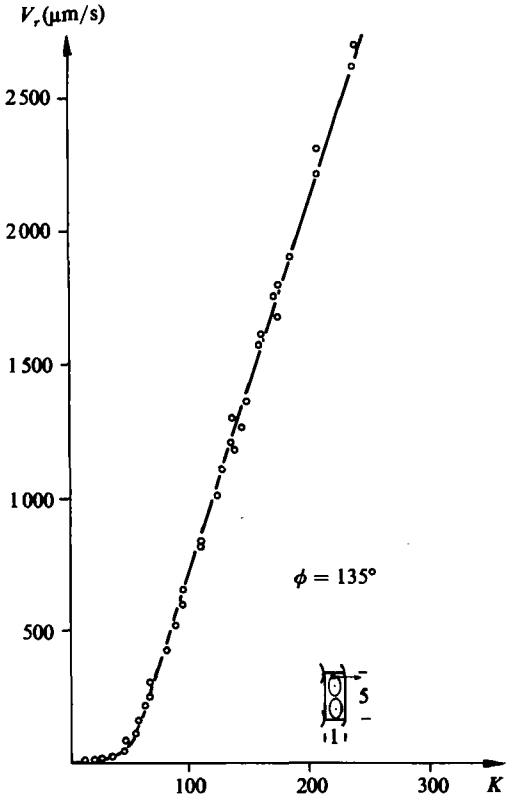


FIGURE 16. The dependence of the maximum secondary-flow velocity $V_r$ in the boundary layer near the upper wall as a function of the Dean number. It was measured in a rectangular channel with aspect ratio $h/w = 5$. The location of the measuring volume is sketched in the figure. The secondary flow from the outer to the inner wall forms a strong boundary layer, yet the boundary-layer thickness is $\frac{1}{10}$ of the channel height $b$.

$\psi^{(2)}_{\max}$ is much greater and presumably would require much more than a 180° curve for the fully developed state to be achieved.

Studies of temperature influence on the curved duct flow, studies of inlet flow development, and the first secondary-flow measurements were made in a rectangular curved duct ($d = 3.33$ cm, $R/d = 5.7$, height/width = 10 cm/2 cm). Figure 15 shows a vertical profile of the streamwise velocity, which was measured in the straight inlet section of the rectangular duct. The comparison with the computed theoretical profile shows a slight asymmetry, which appears at a Rayleigh number around 20000.

In the curved section the centrifugal force is reduced only near the upper and lower wall of the curved section. Therefore the secondary-vortex backflow near the upper and lower wall forms a localized jet. The maximum velocity as a function of the Dean number is shown in figure 16; this result also refers to the rectangular duct.

## 4. Onset of the secondary-vortex pair in relation to instability theory

A critical Dean number is often quoted for the appearance of the second vortex pair. This may be taken to suggest that this phenomenon is an instability. We would like to point out that this association is questionable in ducts of square cross-section, since there is no breaking of an invariance or symmetry. For comparison, in infinitely high curved channels there is translational invariance in the $z$-direction, which will indeed be broken at the critical Dean number (Dean 1928*a*).

According to bifurcation theory (Benjamin 1978) an instability in a system with finite height is recognized by branching of flow solutions at a given parameter (Reynolds-number) value. The difference of the numbers of stable and unstable flow solutions must be equal before and after the critical parameter value, i.e. the critical Dean number. The experimentalist has to observe that the number of stable flow solutions changes at the critical Dean number. If the flow is unique up to the critical Dean number, then we can recognize more than one stable flow solution beyond the critical Dean number. For example, the two-vortex solution changes into a two- and a four-vortex state at $K = K_c$. The analogy with competing two- and four-vortex states in the Taylor-flow problem suggests that the transition between such states in curved ducts with finite aspect ratio may be a transcritical bifurcation, i.e. associated with hysteresis. The theoretical results of Nandakumar & Masliyah (1982) for curved pipes may be discussed in this context. They found a bifurcation and a branching of a two-vortex flow solution into a two- and four-vortex flow solution. The appearance and the location of the additional vortex pair found in their calculations are in agreement with the location and the onset Dean number of our second vortex pair. However, the required second flow solution, a two-vortex state, was not found in our experiments. Instead we found a smooth transition from two to four vortices. It may be that the additional two-vortex state can only be reached by a large perturbation which involves not just the developed flow but the flow-development region as well. No evidence for a second flow pattern was found in our experiments (square duct) so that the question of whether the flow structure is subject to a bifurcation remains unanswered.

The following consideration shows that the appearance of an additional vortex pair may result from a stream function that is asymmetric around the line $x = 0$. This asymmetry also occurs in the streamwise velocity profiles, and is, as we will point out, not only a result of geometry. This asymmetry around $x = 0$ is generated by the nonlinear interaction terms, (11)–(14). The stream functions of the first and additional vortex pairs have different symmetries around $x = 0$. Also, the pressure-generated

streamwise velocity and the streamwise velocity induced by the first vortex pair have different symmetries around $x = 0$. While the streamwise flow is even around $z = 0$, the stream function is odd around $z = 0$.

The equations for the mainstream velocity and secondary-flow stream function of fully developed flow large curvature ratios $R/d$ may be written as follows:

$$\left.\begin{aligned} &\frac{\partial V_\phi}{\partial t}+\frac{\partial}{\partial z}\psi\frac{\partial}{\partial x}V_\phi-\frac{\partial}{\partial x}\psi\frac{\partial}{\partial z}V_\phi+\frac{1}{R}\frac{\partial\psi}{\partial z}V_\phi=\nu\Delta V_\phi-\frac{1}{R\rho}\frac{\partial P}{\partial\phi},\\ &\frac{\partial}{\partial t}\Delta\psi+\frac{\partial}{\partial z}\psi\frac{\partial}{\partial x}\Delta\psi-\frac{\partial}{\partial x}\psi\frac{\partial}{\partial z}\Delta\psi=\nu\Delta\Delta\psi+\frac{1}{R}\frac{\partial}{\partial z}V_\phi^2, \end{aligned}\right\} \tag{6}$$

where $$\Delta\Delta\equiv\frac{\partial^4}{\partial x^4}+2\frac{\partial^2}{\partial x^2}\left(\frac{\partial^2}{\partial z^2}\right)+\frac{\partial^4}{\partial z^4},\quad \Delta\equiv\frac{\partial^2}{\partial x^2}+\frac{\partial^2}{\partial z^2},$$

with the boundary conditions

$$V_\phi(x,z)=0;\quad \psi(x,z)=0;\quad \nabla\psi(x,z)=0\quad \text{at } x,z=\pm\tfrac{1}{2}d, \tag{7}$$

where $$\nabla\equiv\left(\frac{\partial}{\partial x},\frac{\partial}{\partial z}\right).$$

Here $\psi$ is the stream function of the secondary flow, $\nu$ is the kinematic viscosity, $P$ is the pressure and $\rho$ is the fluid density. In (6) we neglect some geometrical terms and simplify $1/(x+R)\approx 1/R$. The stream function for the fully developed flow may be expanded in terms of eigenfunctions,

$$\psi(x,z)=\sum_{n,m}C_{m,2n+1}\psi_{m,2n+1}(x,z),\quad n,m=0,1,\ldots, \tag{8}$$

which satisfy the eigenvalue equation

$$\Delta\Delta\psi_{m,2n+1}=\lambda^4_{m,2n+1}\psi_{m,2n+1} \tag{9}$$

and the boundary conditions (7). Here $m$ denotes the number of nodes of the eigenfunctions $\psi_{m,2n+1}$ in the $r$-direction and $2n+1$ the number of nodes in $z$-direction, the latter being odd for symmetry reasons. The coefficients $C_{m,2n+1}$ satisfy an infinite number of nonlinear coupled ordinary differential equations which result from (6).

The eigenfunction representing the stream function of the primary vortex pair is $\psi_{0,1}$. We want to denote the function $\psi_{0,1}$ and its harmonics as $\psi_{\mathrm{s,a}}$, indicating a symmetry about $x = 0$ and antisymmetry about $z = 0$. The eigenfunction representing four vortices in four corners is $\psi_{1,1}$. We want to denote $\psi_{11}$ and its harmonics as $\psi_{\mathrm{a,a}}$. A linear superposition of the introduced functions $\psi_{\mathrm{a,a}}$ and $\psi_{\mathrm{s,a}}$ leads to a secondary flow field with first and additional vortex pairs which depends on the ratio $C_{1,1}/C_{0,1}$ and on the sign of these expansion coefficients. We may also evaluate the streamwise flow component $V_\phi$ in terms of eigenfunctions $V^\phi_{i,j}$ according to

$$\left.\begin{aligned} &\Delta V^\phi_{i,j}=-\lambda^2_{i,j}V^\phi_{i,j}\\ \text{with}\quad &V_\phi=0\quad \text{at } x,z=\pm\tfrac{1}{2}d. \end{aligned}\right\} \tag{10}$$

In this case $V^\phi_{0,0}$ and harmonics represents a straight channel flow $V^\phi_{\mathrm{s,s}}$. The streamwise flow, which is asymmetric about $x = 0$, $V^\phi_{\mathrm{a,s}}$, is obviously the result of the interaction between primary and secondary flows:

$$V^{\mathrm{i}}_{\mathrm{a,s}}=\frac{\partial}{\partial z}\psi_{\mathrm{a,a}}\frac{\partial}{\partial x}V^\phi_{\mathrm{a,s}}-\frac{\partial}{\partial x}\psi_{\mathrm{a,a}}\frac{\partial}{\partial z}V^\phi_{\mathrm{a,s}}+\frac{\partial}{\partial z}\psi_{\mathrm{s,a}}\frac{\partial}{\partial x}V^\phi_{\mathrm{s,s}}-\frac{\partial}{\partial x}\psi_{\mathrm{s,a}}\frac{\partial}{\partial z}V^\phi_{\mathrm{s,s}}, \tag{11}$$

and there is a smaller-magnitude term due to geometric properties:

$$V^{\mathrm{g}}_{\mathrm{a,s}} = \frac{\partial}{\partial z}\psi_{\mathrm{s,a}}\, V^{\phi}_{\mathrm{a,s}}\, \frac{1}{R}. \tag{12}$$

The secondary flow is generated by the centrifugal force,

$$\psi^{\mathrm{c}}_{\mathrm{a,a}} = \frac{2}{R}\frac{\partial}{\partial z}(V^{\phi}_{\mathrm{a,s}}\, V^{\phi}_{\mathrm{s,s}}), \quad \psi^{\mathrm{c}}_{\mathrm{s,a}} = \frac{1}{R}\frac{\partial}{\partial z}(V^{\phi^2}_{\mathrm{s,s}} + V^{\phi^2}_{\mathrm{a,s}}), \tag{13a,b}$$

and by self-interaction of the secondary flow,

$$\psi^{\mathrm{i}}_{\mathrm{a,a}} = \frac{\partial}{\partial z}\psi_{\mathrm{s,a}}\frac{\partial}{\partial x}\Delta\psi_{\mathrm{s,a}} - \frac{\partial}{\partial x}\psi_{\mathrm{s,a}}\frac{\partial}{\partial z}\Delta\psi_{\mathrm{s,a}} + \frac{\partial}{\partial z}\psi_{\mathrm{a,a}}\frac{\partial}{\partial x}\psi_{\mathrm{a,a}} - \frac{\partial}{\partial x}\psi_{\mathrm{a,a}}\frac{\partial}{\partial z}\Delta\psi_{\mathrm{a,a}}, \tag{14a}$$

$$\psi^{\mathrm{i}}_{\mathrm{s,a}} = \frac{\partial}{\partial z}\psi_{\mathrm{a,a}}\frac{\partial}{\partial x}\Delta\psi_{\mathrm{s,a}} - \frac{\partial}{\partial x}\psi_{\mathrm{s,a}}\frac{\partial}{\partial z}\Delta\psi_{\mathrm{a,a}} + \frac{\partial}{\partial z}\psi_{\mathrm{s,a}}\frac{\partial}{\partial x}\Delta\psi_{\mathrm{a,a}} - \frac{\partial}{\partial x}\psi_{\mathrm{a,a}}\frac{\partial}{\partial z}\Delta\psi_{\mathrm{s,a}}. \tag{14b}$$

The generation of the second vortex pair depends on the magnitude of $\psi_{\mathrm{a,a}}$ in relation to $\psi_{\mathrm{s,a}}$. From (13) and (14) it is obvious that $\psi_{\mathrm{a,a}}$ is generated by $V^{\phi}_{\mathrm{a,s}}$ and $V^{\phi}_{\mathrm{s,s}}$. Because $V^{\phi}_{\mathrm{a,s}}$ is always induced by a first vortex pair $\psi_{\mathrm{s,a}}$, (11), we may conclude that $\psi_{\mathrm{a,a}}$ is always generated.

Now, for a given $C_{0,1}$, which represents $\psi_{\mathrm{s,a}}$ or the first vortex pair, and small $C_{1,1}$, which represents $\psi_{\mathrm{a,a}}$, the resulting stream function is that of a two-vortex system, but with the symmetry about $x = 0$ removed. A four-vortex state can be recognized only if the ratio $C_{1,1}/C_{0,1}$ reaches a certain magnitude. The most likely ('generic') expectation is that both $C_{0,1}$ and $C_{1,1}$ increase monotonically, although at a different rate, as functions of the Reynolds number. Then there is no good reason to call the first measurable appearance of the additional vortex pair a bifurcation, since in that vicinity the significant parameters change smoothly and monotonically.

## 5. Comparison with computer results and conclusions

Table 1 shows results of computer calculations by Ghia & Sokhey (1977), Joseph *et al.* (1975) and Cheng *et al.* (1976), together with some of our measured results. The data do not allow a quantitative comparison in every respect, since vastly different curvature ratios were used. Nevertheless, some qualitative agreement is found. All authors state that the second vortex pair exists only in the range $K_1 < K$, where $K_1$ is uncertain by a factor of 2 at the most. The values $\psi^{(1)}_{\max}$ of the stream-function maximum of the dominant vortex pair in the computed results by Ghia & Sokhey (1977) and Joseph *et al.* (1975) are similar to the experimental ones, whereas the computations of Cheng *et al.* (1976) yield for $\psi^{(1)}_{\max}$ values greater by a factor of 2. Cheng *et al.* also computed a high value 16.7 for $\psi^{(2)}_{\max}$.

All our measured $\psi^{(2)}_{\max}$ values are lower than computer results by a factor of 2–4. From figure 14 it is obvious that the strength of the second vortex pair increases with azimuthal angle. Therefore we conclude that the vortex strength of the second vortex pair would continue to increase in a helically coiled tube for azimuthal angles $\phi > 180°$. If we extrapolate figure 14 to beyond 180°, $\psi^{(2)}_{\max}$ would be increased by about 1 for $\Delta\phi = 36°$. A vortex strength of 7, which is predicted by Joseph *et al.* (1975), would be reached after $\phi = 300°$, and a vortex strength of 5 (Ghia & Sokhey 1977) would be reached after $\phi = 230°$. This indicates that a 180° bend does not allow for fully developed flow at our curvature ratio $d/R = 1/6.45$. For larger angles the strength of the second vortex pair would presumably increase until it reaches the value predicted for developed flow.

| Authors | | JS | GS | PM | CL | JS | GS | PM | JS | CL | CL | PM | CL |
|---|---|---|---|---|---|---|---|---|---|---|---|---|---|
| Dean number | $K$ | 58 | 55 | 80 | 151 | 152 | 143 | 226 | 345 | 368 | 488 | 334 | 520 |
| Curvature ratio | $R/d$ | 10 | 14 | 6.45 | 100 | 5 | 36 | 6.45 | 10 | 10 | 4 | 6.45 | 4 |
| Reynolds number | $Re$ | 182 | 206 | 203 | 1510 | 339 | 858 | 574 | 1091 | 1164 | 976 | 853 | 1040 |
| Stream function, first vortex pair | $\psi_{\max}^{(1)}$ | 3 | 3.6 | 5 | 9.8 | 5,5 | 6.0 | 9 | 10 | 18.2 | 21.8 | 10 | 47.1 |
| Stream function second vortex pair | $\psi_{\max}^{(2)}$ | — | * | * | * | 5,0 | 5.0 | 1...3.5 | 7 | 13.5 | 16.7 | * | * |

*Notes*:

JS, Joseph *et al.* (1975), results related to hydraulic diameter; GS, Ghia & Sokhey (1977); CL, Cheng *et al.* (1976); PM, present measurements; *, no indication of second vortex pair in calculation or measurement.

TABLE 1. Comparison between experimental and numerical results. Qualitative agreement was found in comparison with Cheng *et al.* (1976). The stream-function values are in rough agreement with our results. The onset of the additional vortex pair, computed by Ghia & Sokhey (1977), $K = 143$, is comparable to $K = 150$ from our results.

Only Humphrey *et al.* (1982) calculated numerically the streamwise flow development and the angular development of secondary vortices in a curved duct. They found the additional vortex pair at a Dean number of 485. This disagrees with our flow measurements at $K = 344$. The reason seems to be the different curvature ratio – Humphrey *et al.* used $d/R = 1/3.35$, while we used $d/R = 1/6.45$.

In summary, our experiments permit the distinction of several phases in flow development.

1. Initially the maximum of the main flow component moves outward between $\phi = 0$ and $\phi = 60°$ owing to a tendency for linear-momentum conservation.

2. Between 45° and 108° the unbalanced mass flux of the first vortex pair causes transport of some streamwise momentum back into the region between the duct centre and the inner wall.

3. Beyond 108° the vortex strength of the first vortex pair is constant and the streamwise velocity between the inner wall and the duct centre remains the same.

4. Between 60° and the outlet an additional vortex pair is generated and grows. For angles $\phi < 108°$ it was not possible to separate the secondary velocities of the additional vortex pair from the secondary velocities induced by the overshoot.

5. The fully developed state is expected to be reached for $\phi > 180°$ – an estimate is 220°. Then the interaction between second vortex pair and streamwise velocity should be constant.

6. The second vortex pair is observed only in the range of Dean numbers $150 < K < 300$ ($d/R = 1/6.45$).

Available evidence suggests that the flow pattern in curved square ducts at these low Reynolds numbers is unique. Considering recent results on hysteresis effects in Taylor–Couette flow (Mullin, Pfister & Lorenzen 1982) and taking the results of Nandakumar & Masliyah (1982) into account, one may surmise that a similar hysteretic bifurcation becomes observable in a curved rectangular channel with height $h$ larger than width $w$. For example, in a channel with appropriate aspect ratio $h/w$, one may expect alternatively two or four vortices. In early experiments with $h/w = 5$ we observed two alternative flow patterns, but were not able to reproduce them.

This work was made possible by financial support from the Deutsche Forschungsgemeinschaft under contract Schu 419. We thank Dipl.-Phys. H. Agustin for his help in setting up controlled thermal and flow conditions. We are grateful to Dr T. Mullin, Oxford, for reading the manuscript.

## REFERENCES

AGRAWAL, Y., TALBOT, L. & GONG, K. 1978 Laser anemometer study of flow development in curved circular pipes. *J. Fluid Mech.* **85**, 497–518.

AUGUSTIN, H. 1982 Realisierung einer nahezu idealen Laminarströmung im Rechteck-Kanal durch Schaffung geeigneter thermischer und hydrodynamischer Bedingungen. Diplomarbeit, Kiel.

BENJAMIN, T. B. 1978 Bifurcation phenomena in steady flows of a viscous fluid. I. Theory. II. Experiment. *Proc. R. Soc. Lond.* A **359**, 1–26, 27–43.

BERGER, S. A., TALBOT, L. & YAO, L. S. 1983 Flow in curved pipes. *Ann. Rev. Fluid Mech.* **15**, 461–512.

BERTELSEN, A. & THORSEN, L. K. 1982 An experimental investigation of oscillatory flow in pipe bends. *J. Fluid Mech.* **118**, 269–284.

CHENG, K. C., HONG, S. W. & HWANG, G. J. 1972 Buoyancy effects on laminar heat transfer in the thermal entrance region of horizontal rectangular channels with uniform wall heat flux for large Prandtl number fluid. *Intl J. Heat Mass Transfer* **15**, 1819.

CHENG, K. C., LIN, R. C. & OU, J. W. 1976 Fully developed flow in curved rectangular channels. *Trans. ASME* I: *J. Fluids Engng* **98**, 41–48.

CHANG, S. M., HUMPHREY, J. A. C. & MODAVI, A. 1983 Turbulent flow in a strongly curved U-bend and downstream tangent of square cross-sections. *Physico-Chem. Hydrodyn.* **4**, 243–269.

CUMMINS, H. Z. & PIKE, E. R. 1977 *Photon Correlation Spectroscopy and Velocimetry*. Plenum.

DEAN, W. R. 1927 Note on the motion of fluid in a curved pipe. *Phil. Mag.* (7) **4**, 208–223.

DEAN, W. R. 1928*a* Fluid motion in a curved channel. *Proc. R. Soc. Lond.* A **121**, 402–420.

DEAN, W. R. 1928*b* The streamline motion of fluid in a curved pipe (second paper). *Phil. Mag.* (7) **5**, 673–695.

DURST, F., MELLING, A. & WHITELAW, J. H. 1976 *Principles and Practice of Laser-Doppler Anemometry*. Academic.

GHIA, K. N. & SOKHEY, J. S. 1977 Laminar incompressible viscous flow in curved ducts of rectangular cross-sections. *Trans. ASME* I: *J. Fluids Engng* **99**, 640–648.

HALL, P. 1982 Centrifugal instabilities of circumferential flows in finite cylinders: the wide gap problem. *Proc. R. Soc. Lond.* A **384**, 359–379.

HILLE, P. 1981 Zur Entwicklung von laminaren Strömungen in gekrümmten Kanälen. Diplomarbeit, Kiel.

HILLE, P., VEHRENKAMP, R. & SCHULZ-DUBOIS, E. O. 1983 Measurement of small secondary flow components by photon correlation velocimetry. *Optica Acta* **30**, 139–153.

HUMPHREY, J. A. C. 1978 Numerical calculations of developing laminar flow in pipes of arbitrary curvature radius. *Can. J. Chem. Engng* **56**, 151–164.

HUMPHREY, J. A. C., CHANG, S. M. & MODAVI, A. 1982 Developing turbulent flow in 180° bend and downstream tangent of square cross-sections. *LBL Rep.* 14844 (Berkeley).

HUMPHREY, J. A. C., TAYLOR, A. M. K. & WHITELAW, J. H. 1977 Laminar flow in a square duct of strong curvature. *J. Fluid Mech.* **83**, 509–527.

JOSEPH, B., SMITH, E. P. & ADLER, R. J. 1975 Numerical treatment of laminar flow in helically coiled tubes of square cross-section. *AIChE J.* **21**, 965–979.

JOSEPH, D. D. 1981 Hydrodynamic stability and bifurcation. In *Hydrodynamic Instabilities and the Transition to Turbulence* (ed. H. L. Swinney & J. P. Gollub), pp. 27–76. Springer.

MCCONALOGUE, D. J. & SRIVASTAVA, R. S. 1968 Motion of a fluid in a curved tube. *Proc. R. Soc. Lond.* A **307**, 37–53.

MORI, Y. & FUTAGAMI, K. 1967 Forced convective heat transfer in uniformly heated horizontal tubes. *Intl J. Heat Mass Transfer* **10**, 1801.

MORI, Y., UCHIDA, V. & UKON, T. 1971 Forced convective heat transfer in a curved channel with a square cross section. *Intl J. Heat Mass Transfer* **14**, 1787–1805.

MULLIN, T. & GREATED, C. A. 1980 Oscillatory flow in curved pipes. *J. Fluid Mech.* **98**, 383–416.

MULLIN, T., PFISTER, G. & LORENZEN, A. 1982 New observations on hysteresis effects in Taylor–Couette flow. *Phys. Fluids* **25**, 1134–1136.

NANDAKUMAR, K. & MASLIYAH, J. M. 1982 Bifurcation in steady laminar flow through curved tubes. *J. Fluid Mech.* **119**, 475–490.

OLSON, D. E. 1971 Fluid mechanics relevent to respiration-flow within curved or elliptical tubes and bifurcating systems. Ph.D. thesis, University of London.

OLSON, D. E. & SNYDER, B. 1982 The growth of swirl in curved circular pipes. *Phys. Fluids* **26**, 347–349.

OU, J. W., CHEN, K. C. & LIN, R. C. 1974 Natural convection effects in horizontal rectangular channels with uniform wall temperature for large *Pr*. *Intl J. Heat Mass Transfer* **17**, 835–843.

SCHLICHTING, H. 1934 Laminare Kanaleinlaufströmung. *Z. angew. Math. Mech.* **14**, 368–373.

SCHEEL, H. J. & SCHULZ-DUBOIS, E. O. 1982 The role of hydrodynamics in crystal growth from high-temperature solutions. In *Convective Transport and Instability Phenomena* (ed. J. Zierep & H. Oertel), pp. 491–513. Braun.

SINGH, P. 1974 Entry flow in a curved pipe. *J. Fluid Mech.* **65**, 517–539.

SMITH, F. T. P. 1976 Fluid flow into a curved pipe. *Proc. R. Soc. Lond.* A **351**, 71–87.

TALBOT, L. & GONG, K. 1983 Pulsatile entrance flow in a curved pipe. *J. Fluid Mech.* **127**, 1–25.

TAYLOR, A. M. K. P., WHITELAW, J. J. & YIANNESKIS, M. 1982 Curved ducts with strong secondary motion – velocity measurements of developing laminar and turbulent flow. *Trans. ASME* I: *J. Fluids Engng* **104**, 350–359.

VEHRENKAMP, R. 1980 Nach dem Photonen-Korrelations-Verfahren durchgeführte Laser-Doppler-Messungen zur Wirbelentstehung in gekrümmten Kanälen. Dissertation, Kiel.

VEHRENKAMP, R. & PFISTER, G. 1980 Advances in the analysis of weak secondary flows. In *Proc. Intl Conf. on Long Range and Short Range Optical Velocity Measurements, St Louis, France.*

VEHRENKAMP, R. 1980 Investigations of hydrodynamic instabilities by photon correlation anemometry. In *Proc. 4th Intl Conf. on Photon Correlation Techniques in Fluid Mechanics, Stanford.*

YAO, L. S. & BERGER, S. A. 1975 Entry flow in a curved pipe. *J. Fluid Mech.* **67**, 177–196.